

Chapter 3:

ATP-Independent Reversal of a Membrane

Protein Aggregate by a Chloroplast SRP Subunit

A version of this chapter has been published as:

Jaru-Ampornpan, P., Shen, K., Lam, V.Q., Ali, M., Doniach, S., Jia, T.Z., and Shan, S. (2010) *Nat. Struct. Mol. Bio.*, **17** (6), 696–702.

K.S., V.Q.L, M.A., and S.D. contributed to the SAXS experiments and analyses in this paper.

Abstract

Membrane proteins impose enormous challenges to cellular protein homeostasis during their post-translational targeting, and require chaperones to keep them soluble and translocation-competent. Here we show that a novel targeting factor in the chloroplast Signal Recognition Particle (cpSRP), cpSRP43, is a highly specific molecular chaperone that efficiently reverses the aggregation of its substrate proteins. In contrast to AAA⁺-chaperones, cpSRP43 utilizes specific binding interactions with its substrate to mediate its disaggregase activity. This “disaggregase” capability can allow targeting machineries to more effectively capture their protein substrates, and emphasizes a close connection between protein folding and trafficking processes. Moreover, cpSRP43 provides the first example of an ATP-independent disaggregase, and demonstrates that efficient reversal of protein aggregation can be attained by specific binding interactions between a chaperone and its substrate.

Introduction

Protein homeostasis, or proteostasis, is essential for all living cells. It requires precise control of the folding of proteins, their interactions, and their proper localization in a cell (1). Central to the proteostasis network is the cooperative action of an elaborate set of molecular chaperones, which ensures productive protein folding and effectively prevents the misfolding and aggregation of proteins (2–4). Once a protein aggregates, however, only a few chaperones have been identified that can reverse this detrimental process. The central players in these “disaggregase” systems are members of the Clp/Hsp104 family of proteins, which share an architecture of hexameric rings assembled from the ATPases associated with various cellular activities (AAA⁺) and use repetitive cycles of ATP binding and hydrolysis to drive disaggregation (5). These disaggregases often collaborate with the Hsp70/40 chaperones to achieve the efficient reversal of protein aggregation (6).

Membrane proteins pose enormous challenges to the maintenance of proper proteostasis during their post-translational transport. En route to their cellular destinations, membrane proteins must traverse aqueous environments in which they are prone to aggregation or misfolding. Therefore protein-targeting machineries, an essential part of the proteostasis network, must provide chaperones to protect their membrane protein substrates from aggregation and to keep them in a translocation-competent state. Examples include SecB that targets outer membrane proteins to the bacterial plasma membrane (7), Skp that chaperones bacterial outer membrane proteins in the periplasmic space (8), Get3/TRC40 that delivers tail-anchored proteins to the endoplasmic reticulum (9), and the mitochondrial import stimulation factor (MSF) or Hsp70 homologues that

deliver mitochondria- and chloroplast-resident membrane proteins (10). These examples underscore an essential link between chaperone function and protein trafficking.

The localization of light-harvesting complexes in chloroplasts represents a major membrane protein targeting pathway in nature. The substrates of this targeting reaction are the light-harvesting chlorophyll *a/b* binding (LHC) family of proteins, of which the most abundant member, LHCP, constitutes roughly 50% of the thylakoid proteins and is likely the most abundant membrane protein on earth (11). LHCP is synthesized in the cytosol and imported into the chloroplast stroma, where it is delivered to the thylakoid membrane by the chloroplast signal recognition particle (cpSRP) (12). cpSRP is a heterodimer (13) of cpSRP54, which interacts with the SRP receptor on the thylakoid membrane (14), and cpSRP43, a unique chloroplast protein. cpSRP43 is replete with domains and motifs that typically mediate protein–protein interactions: four ankyrin repeats (A1–A4) and three chromodomains (CD1–CD3) (15–17). The ankyrin repeats have been implicated in LHCP recognition (18,19), CD2 interacts with the cpSRP54 M-domain (20), whereas the functions of CD1 and CD3 remain elusive.

LHCP is a highly hydrophobic protein as it is comprised primarily of three transmembrane helices, and its proper folding and assembly require the hydrophobic environment provided by the thylakoid membrane and the binding of 18 photosynthetic pigments at its core (21–23) (Figure 3.1A). Thus in the aqueous environment of the stroma, it is essential to keep LHCP in a soluble, translocation-competent form. Based on the observation of a soluble “transit complex” between LHCP and cpSRP in native gels, cpSRP has been implied to provide a chaperone that maintains the solubility of

LHCP (12). It was further suggested that cpSRP54 binds to the third transmembrane helix of LHCP (13), whereas cpSRP43 binds a highly conserved stretch of 18 amino acids (L18, Figure 3.1A, pink) preceding the third transmembrane domain of LHCP (24, 25). Nevertheless, the potency of cpSRP as a molecular chaperone, the subunit(s) responsible for its chaperone activity, and its mechanism of action have remained unclear.

Here we show that cpSRP43 is a specific and highly effective molecular chaperone for the LHC family of proteins. Importantly, cpSRP43 not only prevents the aggregation of LHCP but also actively re-solubilizes existing LHCP aggregates. In contrast to chaperones built from AAA⁺-ATPases, cpSRP43 uses specific and extensive binding interactions with its substrate to propel the efficient reversal of protein aggregation. These findings demonstrate that a cellular targeting factor could be highly effective at overcoming protein aggregation problems, and that efficient protein disaggregation can be achieved by a small and simple protein fold.

Materials and Methods

Protein expression and purification. Mature cpSRP43, cpSRP54, and cpFtsY were expressed and purified as described (18, 26). cpSRP43-R161A and cpSRP43-Y204A were constructed using the QuikChange procedure (Stratagene), and were expressed and purified as wild-type protein. All deletion mutants of cpSRP43 were cloned between the BamHI and XhoI restriction sites in pGEX-4T-3 (GE Healthcare). The protein segment corresponding to each deletion mutant has been described (17, 18). The GST fusion proteins were expressed in BL21 (DE3)* cells and purified with Glutathione-S-sepharose (GE Healthcare) in PBS buffer. After Thrombin cleavage, the resulting cpSRP43 proteins were further purified using a MonoQ column (GE Healthcare). Mutant LHCPs, Δ DPLG and L164K, were constructed using the QuikChange procedure. LHCA1 and LHCB5 were subcloned into pQE-80L (Qiagen). All LHCP variants were expressed as His-tagged proteins in BL21 (DE3)* cells as described (27). Inclusion bodies containing recombinant LHCP were purified with Ni-NTA resins (Qiagen) under denaturing condition with 8 M urea.

Sedimentation assay. All measurements were performed in Buffer D [50 mM KHEPES (pH 7.5), 200 mM NaCl]. All reactions contained a final concentration of 5 μ M LHCP and 10 μ M chloroplast proteins. After incubation at room temperature for ten minutes, the mixtures were centrifuged at top speed in a microfuge, and soluble and pellet fractions were analyzed by SDS-PAGE.

Light scattering assay. Measurements were performed in Buffer D on a Beckman DU-640 spectrophotometer. A final concentration of 1 μ M LHCP was used except when otherwise specified. To analyze prevention of LHCP aggregation, urea-denatured LHCP

(or variants) was diluted into buffer with or without chaperone proteins and the absorbance at 360 nm was recorded for five minutes. The absorbance readings were normalized to that of the sample with no chaperone in side-by-side experiments. Time traces shown are representative of three or more side-by-side experiments. Error bars denote standard deviations from three or more experiments. To analyze reversal of LHCP aggregation, urea-denatured LHCP was allowed to aggregate in buffer for 30 seconds. Chaperone proteins were then added and the measurement continued for ten minutes. All absorbance readings were normalized to that at $t=30$ s for the reaction that received no chaperone. The disaggregation time courses were fit to eq 1,

$$A = A_f + \Delta A e^{-k_{obsd}t} \quad (1)$$

in which A is the observed light scattering, A_f is the amount of light scattering at $t \rightarrow \infty$, ΔA is the extent of light scattering change, and k_{obsd} is the observed rate constant to reach equilibrium. The forward disaggregation rate constants, k_f (Figure 3.4F), were obtained from the values of k_{obsd} and ΔA as described in Supplementary Note. The concentration dependence of k_f was fit to eq 2,

$$k_f = k_0 \times \frac{K_d^n}{K_d^n + [cpSRP43]^n} + k_1 \times \frac{[cpSRP43]^n}{K_d^n + [cpSRP43]^n} \quad (2)$$

in which k_0 is the rate of spontaneous LHCP disaggregation in the absence of the chaperone, K_d is an average equilibrium dissociation constant for binding of cpSRP43 to LHCP aggregates, and n is the Hill coefficient.

Kinetic simulations. Kinetic simulations were performed with Berkeley-Madonna, version 8.2.3 (R. I. Macey, G. F. Oster, University of California at Berkeley). Details of the simulation are described in Supplementary Note.

Fluorescence anisotropy. LHCP were labeled with fluorescein-5'-maleimide (Invitrogen) in denaturing conditions [8 M urea, 50 mM K-HEPES (pH 7.0), 5 mM EDTA]. The labeling efficiency was typically 25–30%. Fluorescence measurements were conducted in SRP buffer [50 mM K-HEPES (pH 7.5), 150 mM KOAc, 2 mM Mg(OAc)₂] using a Fluorolog 3-22 spectrofluorometer (Jobin Yvon). Labeled LHCP (100 nM) was diluted into buffer containing different concentrations of chloroplast proteins. The samples were excited at 450 nm and the fluorescence anisotropy was recorded at 524 nm. The data were fit to eq 3,

$$A_{obsd} = A_0 + \Delta A \times \frac{[LHCP] + [pro] + K_d - \sqrt{([LHCP] + [pro] + K_d)^2 - 4 \times [LHCP][pro]}}{2 \times [LHCP]} \quad (3)$$

in which [pro] is the chaperone concentration, A_{obsd} is the observed anisotropy value, A_0 is the anisotropy value at [pro] = 0, ΔA is the total change in anisotropy, and K_d is the equilibrium dissociation constant.

LHCP translocation assay. Translocation assay is based on protease protection of ³⁵S-labeled LHCP when it is properly integrated into the thylakoid membrane and was performed as described (27). The reactions contained 1 μM cpSRP43 (or its variants), 1 μM cpSRP54, 1 μM cpFtsY (except in the last lane), 1 mM GTP, 1 mM ATP, and salt-washed thylakoid membrane. The integration efficiency was quantified from the intensity of radioactive bands using ImageQuant and normalized to the reaction of wild-type cpSRP43.

SAXS. SAXS measurements were performed at beamline 12-ID at the Advanced Photon Source, Argonne National Laboratory (Argonne, IL) with the X-ray energy set at 12 keV. Data were averaged from five exposures (0.2 seconds) at 25 °C using a sample-detector

distance of 2 meters. Background from buffer [20 mM K-HEPES (pH 7.5), 150 mM KOAc, 150 mM NaCl, 1.5 mM Mg(OAc)₂, 2 mM DTT] was subtracted, and no radiation damage was observed (data not shown). The SAXS data acquired at three different cpSRP43 concentrations showed overlapping Kratky plots (Supplementary Figure 3.S7A), and Guinier analysis of the scattering profile yielded a radius of gyration of 33±1 Å at all protein concentrations, indicating the high quality of data and the absence of aggregation or inter-particle interference.

For the SAXS data obtained at 200 µM cpSRP43 (Figure 3.8A, blue), the program GNOM was used to calculate the intramolecular distance distribution $P(r)$. This provided the input for molecular dynamics simulations using DAMMIN and GASBOR (28, 29) to reconstruct a dummy atom model. Ten independent simulations were performed using each software, and all the runs generated the same overall shape. The results were filtered and averaged using SUPCOMB and DAMAVER (30, 31). The filtered models from different simulation software converged on the same shape. The surface map was obtained with Situs (32, 33) and visualized with Chimera (34). Rigid-body docking of the structures of individual fragments of cpSRP43 into the surface map was performed manually based on their shape and the connections between the C- and N-termini of adjacent fragments. The surface map calculated from the molecular model was close to that from the dummy atom model (Supplementary Figure 3.S7B).

Results

cpSRP43 prevents LHCP aggregation.

Previous work suggested that cpSRP can maintain the solubility of LHCP, based on the ability of a ~ 200 kDa complex, comprised of both cpSRP subunits and LHCP, to migrate into native gels. Nevertheless, the majority of LHCP still deposited as insoluble aggregates, indicating a low efficiency of reconstitution (12). We optimized the reconstitution by: (i) using buffer conditions under which cpSRP43 is most active at interacting with LHCP (Supplementary Note and Supplementary Figure 3.S1); and (ii) presenting urea-denatured LHCP (see Methods) as a defined substrate for cpSRP. The latter strategy was based on the consideration that LHCP enters the chloroplast via two translocases on the chloroplast envelope, both of which translocate unfolded polypeptides (35), and that the proper folding and assembly of LHCP require photosynthetic pigments in the thylakoid membrane (22, 23). Thus, the substrate for cpSRP is most likely a largely unfolded LHCP molecule.

Using a sedimentation assay, we found that virtually all LHCP aggregated in aqueous buffer (Figure 3.1B, lane 1). A twofold molar excess of cpSRP allowed almost all the LHCP to be retained in the soluble fraction (Figure 3.1B, lane 4), demonstrating robust reconstitution of cpSRP's chaperone activity. Consistent with previous observations (25), cpSRP54 alone could not prevent the aggregation of LHCP (Figure 3.1B, compare lanes 6 and 7). To our surprise, cpSRP43 alone could retain LHCP in the soluble fraction, suggesting that cpSRP43 has the ability to chaperone LHCP by itself.

To independently test this conclusion, we used light scattering to monitor formation of high-molecular-weight LHCP aggregates in real time. LHCP aggregated

extensively when it was diluted from urea into aqueous buffer; the aggregation was rapid and close to completion during manual mixing (Figure 3.1C). The light-scattering intensity at equilibrium correlated linearly with LHCP concentration (Figure 3.1C and D), indicating that this assay quantitatively measures the amount of aggregates in our experimental range. LHCP aggregation was reduced ~ 80% when urea-solubilized LHCP was diluted into a solution containing equimolar cpSRP (Figure 3.1E, blue vs. black). Higher concentrations of cpSRP completely suppressed LHCP aggregation (Figure 3.1F, blue). Consistent with results from the sedimentation assay, cpSRP43 prevented LHCP aggregation as efficiently as cpSRP (Figure 3.1E and F, green vs. blue), whereas cpSRP54 did not (Figure 3.1E and F, red). Neither cpFtsY, the chloroplast SRP receptor, nor BSA suppressed LHCP aggregation (Figure 3.1E), further suggesting that the chaperone activity stemmed specifically from cpSRP43. These results indicate that cpSRP43 is primarily responsible for maintaining the solubility of LHCP, whereas cpSRP54 exhibits no significant chaperone activity by itself.

cpSRP43 binds LHCP with high affinity.

To quantitatively characterize the binding interactions between cpSRP and its substrate, we labeled a native cysteine (C79) in LHCP with fluorescein-5'-maleimide. Binding of cpSRP or cpSRP43 was detected as an increase in the fluorescence anisotropy of fluorescein-labeled LHCP (Figure 3.2A); this anisotropy change was competed by the L18 peptide (Figure 3.2B), suggesting that it is specific to the LHCP–cpSRP complex. Equilibrium titrations based on this anisotropy change were consistent with 1:1 binding between cpSRP and LHCP, and showed that LHCP bound to cpSRP with an apparent

dissociation constant (K_d) of 97 nM (Figure 3.2A, blue). This is likely an upper limit for the true K_d value of cpSRP–LHCP binding, as a small fraction of LHCP possibly aggregated prior to the addition of cpSRP. Importantly, cpSRP43 bound LHCP with an apparent K_d of 138 nM, close to that observed with cpSRP (Figure 3.2A, green). In contrast, neither cpSRP54 nor cpFtsY by themselves induced significant anisotropy changes (Figure 3.2A, red and gold). Together, the results of this and previous sections demonstrate that cpSRP43 is sufficient for high affinity binding between cpSRP and its substrate. As suggested previously, cpSRP54 may contribute additional binding interactions for LHCP (36); these interactions could be transient in nature, or did not result in a net increase in overall binding affinity to LHCP.

cpSRP43 provides a chaperone for the LHC protein family.

We next tested the ability of cpSRP43 to chaperone other members of the LHCP family including LHCA1 and LHCB5, two close homologues of LHCP (Lhcb1 gene product) (37). Both of these proteins aggregated upon dilution from urea into aqueous buffer, although LHCB5 aggregated more slowly and to a lesser extent than LHCP or LHCA1 (Figure 3.3A and B). In the case of LHCA1, equimolar cpSRP43 could partially help prevent its aggregation whereas equimolar cpSRP suppressed aggregation more efficiently (Figure 3.3A). In the case of LHCB5, equimolar cpSRP43 or cpSRP completely prevented aggregate formation (Figure 3.3B). Thus cpSRP43 can chaperone different members of the LHC protein family and, with more challenging substrates such as LHCA1, cpSRP54 could enhance the chaperone activity of cpSRP43, although cpSRP54 by itself could not chaperone these proteins (data not shown).

cpSRP43 actively reverses LHCP aggregation.

AAA⁺-chaperones such as ClpB and Hsp104 exhibit the ability to re-solubilize protein aggregates (5). To test if cpSRP43 can reverse the aggregation of LHCP, we changed the order of addition and allowed LHCP to aggregate upon dilution from 8M urea into aqueous buffer. cpSRP or cpSRP43 was then added when the aggregation was close to completion (Figure 3.4A). Surprisingly, a twofold excess of cpSRP allowed LHCP to partition back into the soluble fraction even after LHCP had already aggregated (Figure 3.4B, compare lanes 4 and 1), and cpSRP43 was sufficient for re-solubilizing the LHCP aggregates (Figure 3.4B, lane 6). As expected, neither cpSRP54 nor BSA reversed LHCP aggregation (Figure 3.4B and data not shown). Thus cpSRP43 not only prevents, but also readily reverses the aggregation of LHCP.

What mechanism underlies this disaggregase activity? Two alternative models could be envisioned. In a passive mechanism, cpSRP43 binds free LHCP molecules that have transiently dissociated from the LHCP aggregate, and prevents them from re-aggregating (Figure 3.4C). Since the aggregation of LHCP (k_{-1}) and the binding between cpSRP and soluble LHCP molecules (k_2) are fast (Figure 3.1C and data not shown), the rate of disaggregation via this mechanism would be rate-limited by the slow dissociation of LHCP from the aggregates (k_1). Therefore, this model predicts that increasing cpSRP43 concentrations would only drive the equilibrium, but would *not* affect the kinetics of LHCP disaggregation (Figure 3.4C, right, and Supplementary Figure 3.S2). Alternatively, cpSRP43 could interact with and remodel the LHCP aggregates, displacing individual LHCP molecules from the aggregate and converting them to soluble

cpSRP43•LHCP complexes (Figure 3.4D). This model predicts that both the equilibrium and rate constants of LHCP re-solubilization will be highly dependent on cpSRP43 concentration (Figure 3.4D, right).

To distinguish between these two possibilities, we followed the disaggregation reaction in real time using the light scattering assay. Addition of increasing amounts of cpSRP43 resulted in increasingly more efficient reversal of LHCP aggregation (Figure 3.4E), and at sufficiently high cpSRP43 concentrations, the disaggregation of LHCP was complete within 200 seconds or less (Figure 3.4E and F). cpSRP43 was able to dissolve the LHCP aggregates with efficiencies that are within twofold of those observed with cpSRP (Supplementary Figure 3.S3). Quantitative analysis of the rate and equilibrium of LHCP disaggregation (Supplementary Note) led to several important conclusions. First, the equilibrium for the disaggregation reaction became more favorable with increasing concentrations of cpSRP43 (Figure 3.4E) and cpSRP (Supplementary Figure 3.S3), consistent with the notion that binding of cpSRP43 prevented LHCP from re-aggregating. Second, the rate constants of disaggregation increased significantly with increasing concentrations of cpSRP43 (Figure 3.4E and F) or cpSRP (Supplementary Figure 3.S3). Third, the disaggregation rate constants exhibit a cooperative dependence on cpSRP43 concentration, with a Hill coefficient of 1.8 (Figure 3.4F and Supplementary Table 3.S1). This suggests that, although each cpSRP43 binds one soluble LHCP molecule (19) (Figure 3.2A), disaggregation requires the cooperative action of more than one cpSRP43 molecule to dislodge LHCP from the aggregates. These results are consistent with predictions from the active mechanism (Figure 3.4D) but could not be accounted for by the passive mechanism (Figure 3.4C and Supplementary Figure 3.S2), and strongly

suggest that cpSRP43 is an effective molecular chaperone that actively dissolves the aggregates formed by its substrate protein.

Specific binding interactions drive chaperone activity.

Most of the known chaperones that reverse protein aggregation are large macromolecular assemblies built from AAA⁺-ATPases and rely on mechanical forces powered by ATP hydrolysis. How does cpSRP43, a small protein with no ATPase sites, efficiently reverse protein aggregation? We reasoned that the AAA⁺-chaperones need to act on a variety of substrates via highly promiscuous interactions, and have not evolved specific and extensive interactions with their substrates during disaggregation (38–40). cpSRP43, on the other hand, is dedicated to the LHC family of proteins. We therefore hypothesized that cpSRP43, instead of being driven by ATP hydrolysis, utilizes specific binding interactions with its substrate to drive its chaperone/disaggregase activity.

Previous work showed that cpSRP43 specifically binds to the L18 motif of LHCP (Figure 3.1A, pink), a sequence highly conserved throughout the LHC protein family (24, 25). The crystal structure of an L18 peptide bound to the CD1–Ank4 fragment of cpSRP43 identified a DPLG motif in L18 as an important binding site for cpSRP43 (19) (Supplementary Figure 3.S4A). We tested the importance of these binding interactions by deleting this motif (Δ DPLG) or introducing a single mutation, L164K, into DPLG. cpSRP43 or cpSRP, even at a tenfold molar excess, could not suppress the aggregation of Δ DPLG (Figure 3.5A and Supplementary Figure 3.S4B). Similarly, the L164K mutation severely disrupted the binding LHCP to cpSRP (Figure 3.5B), and abolished the ability of cpSRP43 or cpSRP to prevent LHCP aggregation (Figure 3.5A and Supplementary

Figure 3.S4B). These results are consistent with previous work that showed that LHCP-L164K failed to integrate into the thylakoid membrane by the cpSRP pathway (19).

Reciprocally, we mutated residues in cpSRP43 that make important contacts to the L18 peptide (19) (R161A and Y204A). cpSRP43-R161A exhibited significantly reduced chaperone activity, requiring a tenfold molar excess to attain the same solubilization of LHCP as equimolar wild-type cpSRP43 (Figure 3.5C). cpSRP43-Y204A completely abolished the ability of cpSRP43 to suppress LHCP aggregation (Figure 3.5C). Similar results were obtained with cpSRP complexes assembled from these cpSRP43 mutants (Supplementary Figure 3.S4C). The defects of these mutant proteins in chaperoning LHCP correlated with their defects in binding LHCP: cpSRP R161A bound LHCP with a K_d value an order of magnitude higher than that of wild-type cpSRP (Figure 3.5D, squares vs. circles), whereas the cpSRP-Y204A mutation more severely disrupted LHCP binding (Figure 3.5D, diamonds). Together, these mutational results demonstrate that cpSRP43 exhibits high specificity for the LHC family of proteins, and that these specific interactions are essential for the chaperone activity of cpSRP43.

Essential roles of chromodomains.

Previous work revealed a highly modular domain structure of cpSRP43, with three CDs and an ankyrin repeat domain between the first and second chromodomains (15–17) (Figure 3.6A). As cpSRP43 is a protein targeting factor, some of these motifs could be used for functions other than chaperoning LHCP. We therefore defined the

minimal domain requirement for the chaperone activity of cpSRP43 by testing cpSRP43 mutants in which the individual structural motifs were systematically deleted.

Deletion of any of the ankyrin repeats in cpSRP43 abolished its ability to prevent LHCP aggregation, indicating that all the ankyrin repeats are required for chaperone activity (Figure 3.6B). Surprisingly, the CD1–Ank4 fragment (Δ CD2 Δ CD3), despite its ability to bind the L18 peptide as well as wild-type cpSRP43 (19), failed to prevent the aggregation of LHCP (Figure 3.6C), suggesting that additional interactions between the chromodomains of cpSRP43 and the remainder of LHCP are essential for the chaperone activity of cpSRP43. While deletion of the first chromodomain abolished the ability of cpSRP43 to suppress LHCP aggregation (Figure 3.6C), mutants in which either the second or the third chromodomain was deleted could prevent and reverse the aggregation of LHCP almost as efficiently as wild-type cpSRP43 (Figure 3.6C and D, and Supplementary Figure 3.S5). Thus, all of the ankyrin repeats and at least one chromodomain on both the N- and C-termini of the ankyrin repeat domain are required to support cpSRP43's chaperone activity.

Consistent with these results, the cpSRP43 deletion mutants that can prevent and reverse LHCP aggregation, Δ CD2 and Δ CD3, exhibited high affinity binding to LHCP, with K_d values within two- to threefold of that of wild-type cpSRP43 (Figure 3.6E; green and gold vs. black). In contrast, Δ CD1 and Δ CD2 Δ CD3 bound to LHCP with much weaker affinities (Figure 3.6E, blue and red). The results in Figures 3.4 and 3.5 demonstrate a strong correlation between the strength of the cpSRP43–LHCP binding interactions and the ability of cpSRP43 to chaperone LHCP, supporting the notion that these binding interactions and chaperone activity are highly coupled. Together with the

observation that full-length LHCP binds cpSRP43 at least 10–20-fold stronger than the L18 peptide, these results further indicate that the interaction of LHCP with cpSRP43 is extensive and involves not only the previously identified contacts between the L18 motif and ankyrin repeats, but also interactions of the transmembrane domains of LHCP and the chromodomains of cpSRP43. Finally, the mutants that failed to efficiently bind and chaperone LHCP exhibited strong defects in the targeting and integration of LHCP to the thylakoid membrane, whereas Δ CD3, which showed no appreciable defect in the chaperone activity, only mildly affected the integration efficiency (Figure 3.7). Although Δ CD2 showed no significant defect in chaperone activity, this deletion mutant could not support translocation because CD2 is required to interact with cpSRP54 (20). These results highlight the essential role of cpSRP43's chaperone activity in maintaining the translocation competence of LHCP.

Structural reconstruction of cpSRP43.

To address how cpSRP43 could provide sufficient surface to bind a substrate of almost its own size, we reconstructed the global structure of cpSRP43 using small-angle X-ray scattering (SAXS). SAXS reports on the global size and shape of macromolecules in solution, and, in combination with molecular dynamics simulations, can generate a global structural model at resolutions of 10–15 Å (41). High quality SAXS data were acquired for cpSRP43 (Figure 3.8A, blue). Based on this SAXS profile, multiple independent molecular dynamics simulations using different software converged on the dummy atom model shown in Figure 3.8B. The reconstruction was further validated by

calculating a theoretical Kratky curve from this model, which overlapped well with the experimental profile (Figure 3.8A, red vs. blue).

The reconstruction revealed cpSRP43 to be an elongated, curved molecule ~ 120 Å in length and ~ 40 Å in sectional diameter (Figure 3.8B), consistent with an earlier suggestion based on analytical ultracentrifugation results (13). This narrow shape allowed us to dock the previously obtained high-resolution structures of the individual fragments (19, 42) successively into the SAXS reconstruction to generate a molecular model for cpSRP43 (Figure 3.8C). The structure of the CD1–Ank4 fragment fit well into the longer arm of the SAXS reconstructed shape; the small curvature in the crystal structure (19) was independently observed in the SAXS model, increasing our confidence in the position and orientation of this fragment. The good fit of the crystal structure of this fragment into the SAXS reconstruction also suggested that no major structural changes in the CD1–Ank4 fragment were induced by CD2 and CD3; therefore, it seems unlikely that the defect of this fragment in binding and chaperoning LHCP (Figure 3.8C and E) stems from an inactive conformation of CD1–Ank4 without the additional chromodomains. CD2 and CD3 were fit into the middle and other end of the reconstructed shape, respectively; their precise orientations could not be assigned at this resolution without further structural or biochemical constraints (Figure 3.8C). Nevertheless, the elongated shape of cpSRP43 revealed by this model suggests that this chaperone could provide extensive surface area for binding its substrate protein despite its small size, and might be well suited to keep the LHCP molecules in an extended, translocation competent conformation.

Discussion

Post-translational targeting of membrane proteins poses enormous challenges to cellular proteostasis and mandates intimate coupling between the transport and chaperone functions of protein-targeting machineries. The high abundance and highly hydrophobic nature of the LHC family of proteins necessitate a highly effective molecular chaperone during their transport. Here we demonstrated that cpSRP43 efficiently fulfills these requirements. Thus, cpSRP provides a robust model system to test the limits of the chaperone capacity of targeting machineries and to understand their mechanism of action.

The ability of cpSRP43 to reverse LHCP aggregation is intriguing; only a few other chaperones, all of which based on AAA⁺-ATPase assemblies, have been demonstrated to effectively reverse protein aggregation (5). The efficiency with which cpSRP43 re-solubilizes LHCP aggregates is on par with those exhibited by the AAA⁺-ATPase machines. In a similar experimental setup, ClpB, with the help of DnaK/DnaJ/GrpE, dissolves protein aggregates with half-times varying from several minutes to a few hours (43, 44). Hsp104, the eukaryotic homologue of ClpB, dissolves heat-aggregated GFP and facilitates its refolding on a time scale of minutes to hours (45). With the help of an adaptor protein MecA, ClpC reverses protein aggregation on a time scale similar to ClpB (46). Here, cpSRP43 at a concentration of 8 μ M or higher completed the disaggregation process within 100–200 seconds. This efficiency is remarkable given that all the other chaperones are massive macromolecular machines of over 600 kDa and rely on mechanical forces powered by ATP hydrolysis to effect their disaggregase activity, whereas cpSRP43 contains no ATPase sites and the minimal functional unit required to support its chaperone activity is \sim 35 kDa, only slightly larger

than its substrate protein. Although a strict comparison of the disaggregase activity between cpSRP43 and other chaperones could not be made due to the largely unknown and possibly different nature of LHCP aggregates compared to those of previously used model proteins, it is evident that cpSRP43 can function as an effective disaggregase for its substrate proteins without any co-chaperone or ATP consumption. Indeed, cpSRP43 could also reverse heat-aggregated LHCP, albeit with less efficiency (Supplementary Figure 3.S6); this suggests that cpSRP43 can re-solubilize LHCP aggregates generated under different conditions, but the physical or chemical nature of the aggregate affects the efficiency with which this chaperone works.

How does a relatively small chaperone such as cpSRP43 efficiently reverse protein aggregation without ATP hydrolysis? Although the precise molecular mechanism remains to be defined, our results here provided several important clues. First, cpSRP43 has established highly specific and extensive interactions with its substrate, using not only its ankyrin repeats to contact the L18 motif of LHCP, but also additional interactions involving its chromodomains and the transmembrane domains of LHCP. The extended structure of cpSRP43 is consistent with the notion that this chaperone could provide extensive binding surfaces for its substrate protein despite its small size. These binding interactions are crucial for supporting the chaperone activity of cpSRP43. Second, the cooperative dependence of the protein disaggregation rate on cpSRP43 concentration strongly suggests that binding of the first cpSRP43 molecule induces conformational changes in the aggregated LHCP so that the second cpSRP43 molecule can bind more strongly. This supports an active role of cpSRP43 in remodeling the LHCP aggregates, and suggests that the binding interactions of cpSRP43 with LHCP induce changes in the

aggregated LHCP molecules that may disrupt their contacts within the aggregate, thereby dislodging LHCP molecules from the aggregate. As a protein-targeting factor, cpSRP43 most likely keeps solubilized LHCP molecules in a largely unfolded, translocation competent state. The thylakoid membrane environment and the binding of chlorophylls eventually drive the proper folding and assembly of LHCP.

The ability of targeting factors to reverse protein aggregation would allow them to more efficiently capture their substrate proteins, and may reflect a more general feature of chaperones involved in post-translational protein targeting, such as SecB, MSF, and Hsp70. Indeed, SecB has been suggested to passively disaggregate proteins by binding to polypeptides that have dissociated from the aggregate (47). MSF likely provides another example in which a protein targeting factor can efficiently reverse aggregation (48). This chaperone restores the import competence of aggregated precursor proteins in an ATP-dependent manner (48), and the observation that aggregated protein substrates stimulate MSF's ATPase activity (49) strongly supports an active mechanism of disaggregation. Analogous to cpSRP43, MSF specifically recognizes the presequence of mitochondrial precursor proteins, and these specific binding interactions play a crucial role in its chaperone activity (49).

To our knowledge, cpSRP43 provides the first example of a simple solution to overcome protein aggregation problems without energy input from ATP. The key difference between the action of cpSRP43 and ATP-driven disaggregases may arise from their different substrate specificity. Most chaperones from the Clp and Hsp family have evolved to bind a variety of substrates via generic hydrophobic interactions, such that they can rescue proteins from aggregation regardless of sequence identity (38–40).

Sacrificing specificity for variety, these chaperones may resort to larger and more elaborate architectures, cooperative action of multiple chaperones, as well as mechanical forces powered by ATP hydrolysis to exert their action. In contrast, cpSRP43 is found only in the chloroplasts of green plants, and its evolution likely coincided with that of its substrates, the LHCPs (11). Thus, cpSRP43 is dedicated to the LHC family of proteins, and hence has established extensive and highly specific binding interactions with its substrates. With adequate binding interactions, cpSRP43 can bypass the massive architecture, the elaborate chaperone network, and the dependence on ATP. Thus, cpSRP43 illustrates a simple principle that efficient reversal of protein aggregation can be attained with a small protein fold and without external energy input, as long as adequate binding interactions are established between a chaperone and its substrate.

Acknowledgements

We thank T.X. Nguyen for help with the LHCP translocation assay, Drs. R. Henry for expression plasmids of cpSRP43 and LHCP, C. Robinson for plasmids encoding LHCA1 and LHCB5, Z. Liu for help and advice with LHCP reconstitution, A. Sim and V. Chu of the Doniach group and D. Herschlag for help and advice with the SAXS experiments, and D.C. Rees, W.M. Clemons, A. Varshavsky, N. Pierce, and members of the Shan laboratory for comments on the manuscript. This work was supported by NIH grant GM078024, and career awards from the Burroughs Wellcome Foundation, the Henry and Camille Dreyfus foundation, the Beckman foundation, and the Packard foundation to S.S., and by NIH program project grant P01-GM-66275 to S.D. and D.H.

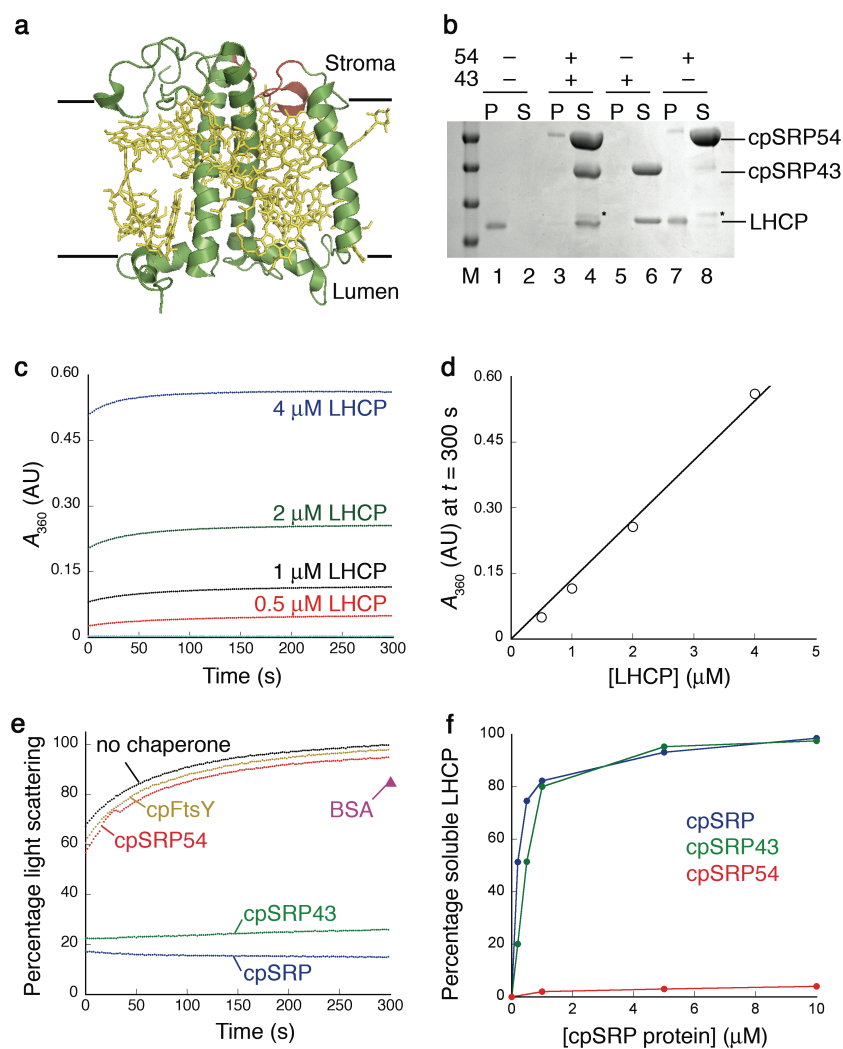


Figure 3.1 cpSRP43 is sufficient for preventing aggregation of LHCP. (A) The crystal structure of an LHCP monomer (21) (PDB ID: 1RWT) in complex with photosynthetic pigments (gold sticks). The black lines depict the thylakoid membrane. Pink highlights the L18 motif. (B) Sedimentation analysis of the ability of cpSRP or its individual subunits to prevent LHCP aggregation. P and S denote the pellet and soluble fractions, respectively. The asterisks mark a small contamination during the preparation of cpSRP54. (C) Time courses for aggregation of LHCP at different starting LHCP concentrations. (D) The light scattering from aggregates is proportional to LHCP concentration. (E) Time courses for LHCP aggregation in the absence (black) or presence of cpSRP (blue), cpSRP43 (green), cpSRP54 (red), or cpFtsY (gold). The magenta triangle represents LHCP aggregation in the presence of BSA. (F) Concentration dependence of LHCP solubilization by cpSRP (blue), cpSRP43 (green), and cpSRP54 (red).

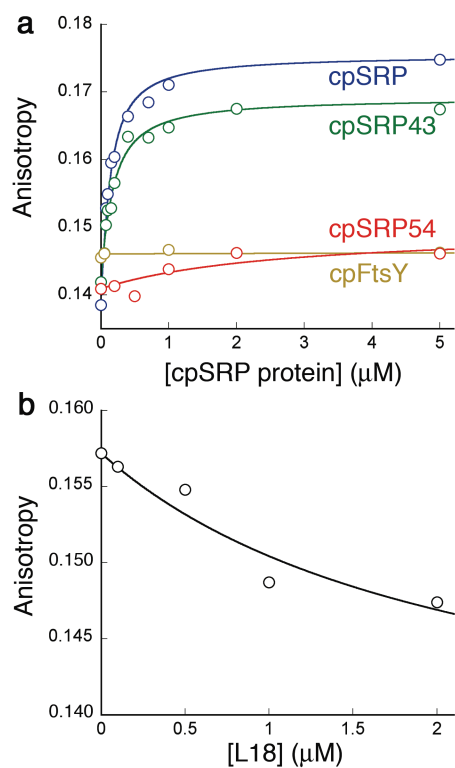


Figure 3.2 LHCP binds with high affinity to cpSRP43. (A) Binding of LHCP to cpSRP components measured by fluorescence anisotropy. The data were fit to eq 3 and gave K_d values of 97 nM for cpSRP (blue) and 138 nM for cpSRP43 (green). cpSRP54 (red) and cpFtsY (gold) showed no significant binding to LHCP. (B) The L18 peptide competes with fluorescein-labeled LHCP in binding to cpSRP43. Nonlinear fit of the data gave an apparent K_i of 2.2 μM , close to the K_d value of the L18–cpSRP43 interaction observed previously (19).

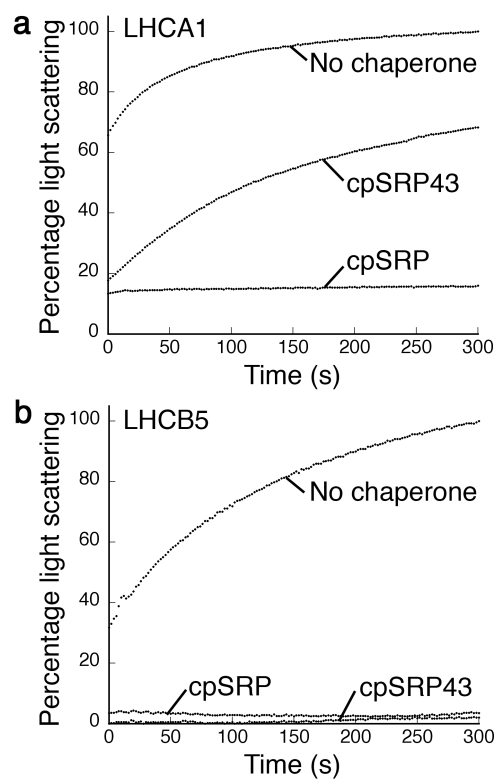


Figure 3.3 cpSRP and cpSRP43 chaperone various members of the LHC family. Time courses for aggregation of LHCA1 (A) and LHCB5 (B) in the absence or presence of equimolar cpSRP or cpSRP43.

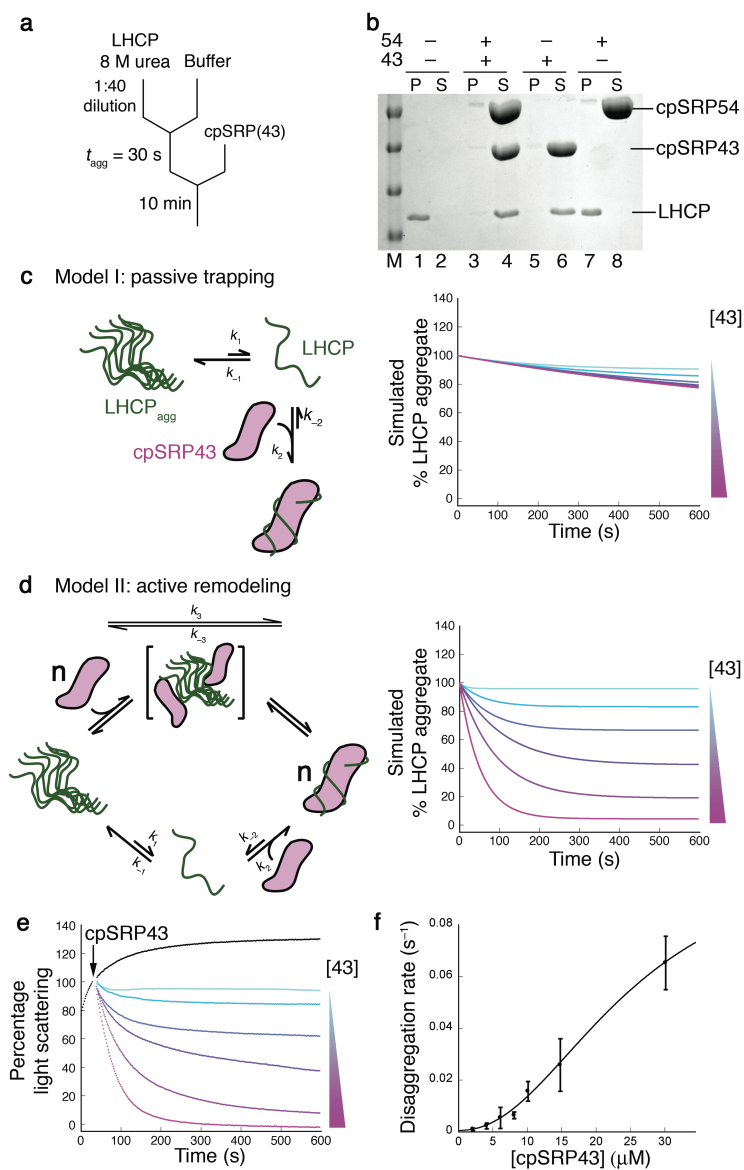


Figure 3.4 cpSRP43 actively reverses LHCP aggregation. (A) Reaction scheme of the disaggregation assay. (B) Sedimentation analysis of LHCP disaggregation by cpSRP or its individual subunits. P and S denote the pellet and soluble fractions, respectively. (C–D) Models for LHCP disaggregation via a passive (C) or an active mechanism (D), as described in text. The right panels show kinetic simulations for each model at varying concentrations of cpSRP43 (see also Supplementary Figure 3.S2) as described in Supplementary Note. (E) Time courses for disaggregation of LHCP (1 μM) at varying concentrations (2–10 μM) of cpSRP43. The black arrow marks the time of cpSRP43 addition. (F) Concentration dependence of the forward rate constants of disaggregation reactions (k_f ; see Methods). Fits to eq 2 gave a Hill coefficient of 1.8.

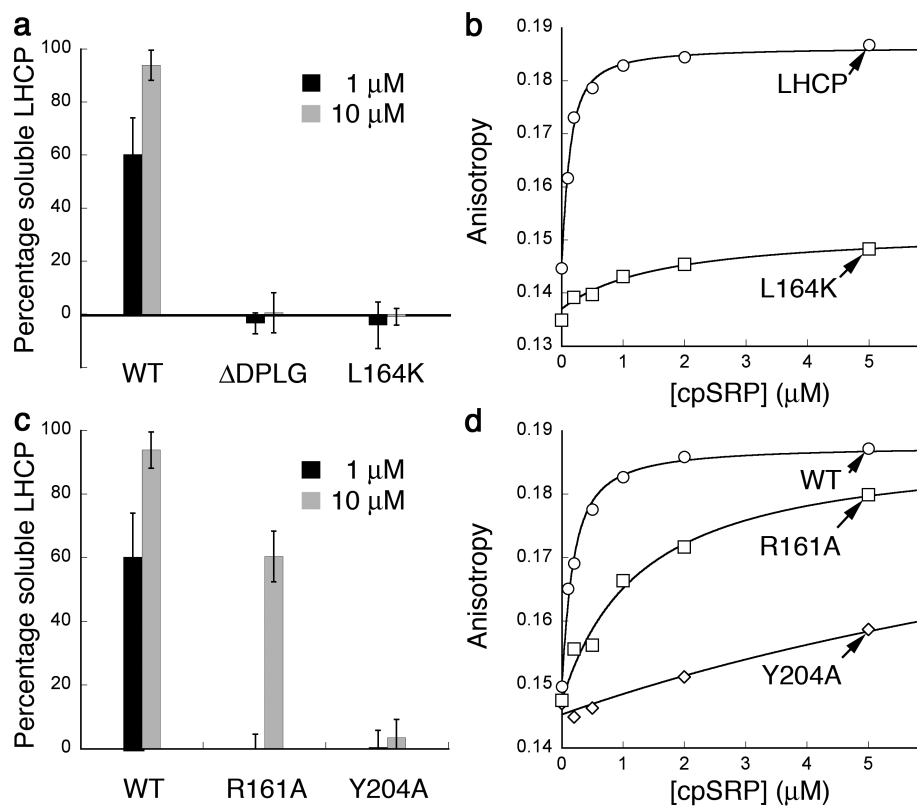


Figure 3.5 Specific binding interactions between LHCP and cpSRP43 are essential for the chaperone activity. (A) The amount of soluble LHCP (1 μM) or its variants, ΔDPLG and L164K, at equilibrium in the presence of 1 μM (black) or 10 μM (gray) cpSRP43. (B) Binding of LHCP (○) and LHCP-L164K (□) to cpSRP. Fits of data to eq 3 gave K_d values of 76 nM for LHCP and $>5 \mu\text{M}$ for L164K. (C) The amount of soluble LHCP (1 μM) at equilibrium in the presence of 1 μM (black) or 10 μM (gray) of cpSRP43 or its mutants, R161A and Y204A. (D) Binding of LHCP to cpSRP (○), cpSRP-R161A (□) and cpSRP-Y204A (◇). Fits of data to eq 3 gave K_d values of 128 nM for wild-type cpSRP, 1.2 μM for cpSRP-R161A, and $>5 \mu\text{M}$ for cpSRP-Y204A.

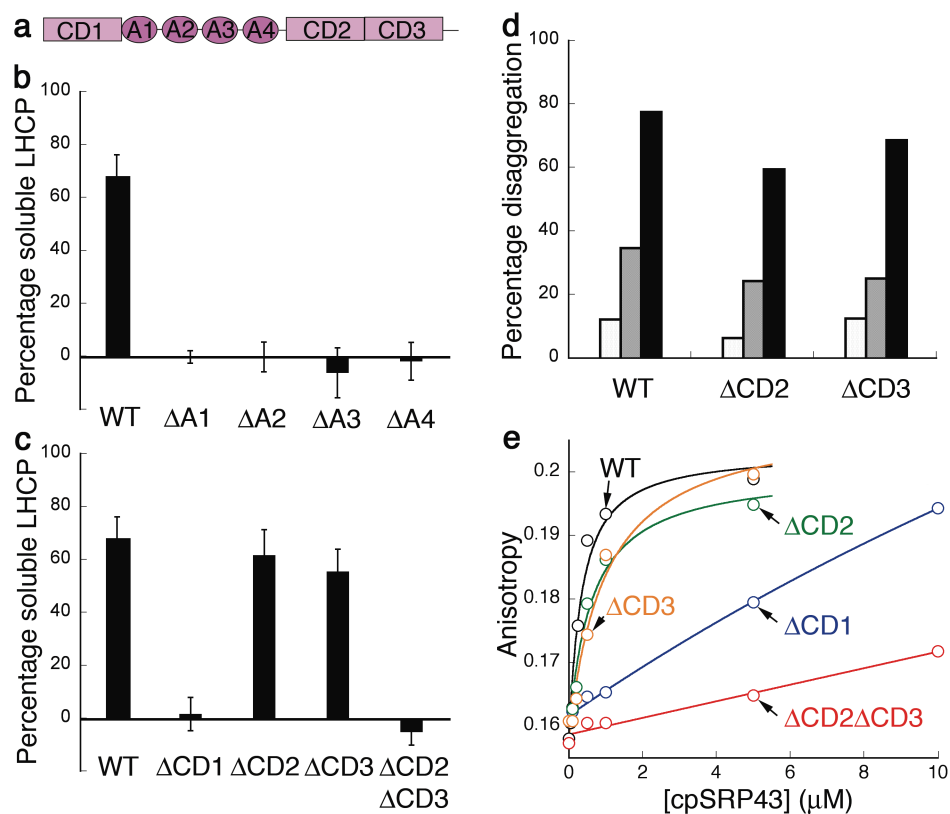


Figure 3.6 Chromodomains are essential for cpSRP43's chaperone activity. (A) Domain composition of cpSRP43. CD denotes the chromodomain, and A1–A4 denotes ankyrin repeats 1–4. (B–C) The amount of soluble LHCP (1 μM) at equilibrium in the presence of 1 μM ankyrin (B) or chromodomain (C) deletion mutants of cpSRP43. (D) The amount of LHCP re-solubilized by 2 (white), 4 (gray), and 8 μM cpSRP43, $\Delta CD2$, or $\Delta CD3$ at equilibrium, obtained from the time courses in Supplementary Figure 3.S5. (E) Binding of LHCP to cpSRP43 (black; $K_d = 296$ nM), $\Delta CD1$ (blue; $K_d > 10$ μM), $\Delta CD2$ (green; $K_d = 530$ nM), $\Delta CD3$ (gold; $K_d = 886$ nM), and $\Delta CD2 \Delta CD3$ (red; $K_d > 10$ μM). K_d values were from fits of data to eq 3.

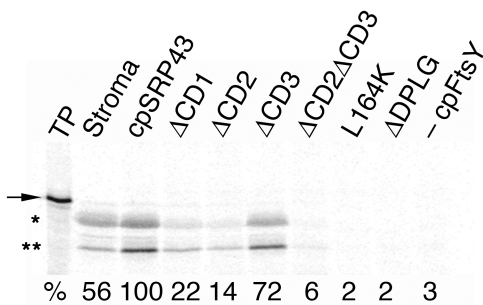


Figure 3.7 cpSRP43 or LHCP mutants defective in chaperone activity could not support LHCP targeting and translocation. The arrow marks full-length LHCP (TP, translation product); the single and double asterisks mark the protected fragments of LHCP that represent products of proper LHCP integration into the thylakoid membrane. The integration efficiency was quantified relative to that of wild-type cpSRP43 and is shown at the bottom.

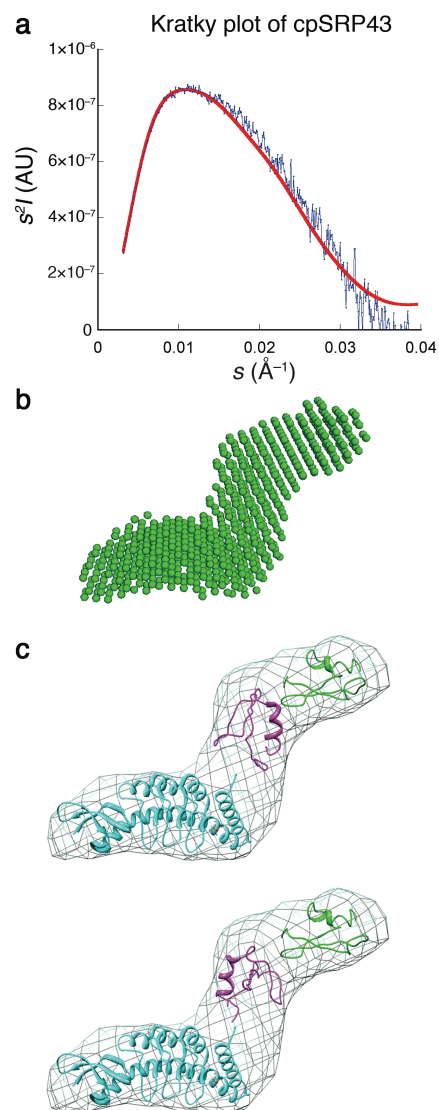


Figure 3.8 SAXS reconstruction of full-length cpSRP43 reveals an elongated shape. (A) Experimental (blue) and theoretical (red) SAXS profiles of cpSRP43 in Kratky's representation. s denotes momentum transfer, and I denotes scattering intensity in arbitrary units. The theoretical curve was calculated from the dummy atom model in B. (B) Dummy atom model of full-length cpSRP43, reconstructed from the SAXS profile as described in Methods. (C) Molecular models generated from rigid-body docking of the structures of individual cpSRP43 fragments into the SAXS reconstructed shape in B. CD1–Ank4 (PDB ID: 3DEO)(19) is in cyan. CD2 (PDB ID: 1X3Q)(42) is in pink. CD3 (PDB ID: 1X3P)(42) is in green. Note that multiple orientations of CD2 and CD3 are possible and cannot be resolved at this resolution; two possible orientations of CD2 are shown here.

Supplementary Materials

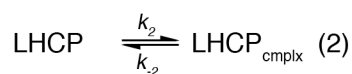
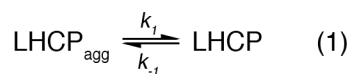
Supplementary Note

Optimization of conditions for reconstituting the LHCP-cpSRP interaction.

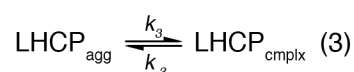
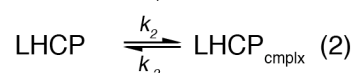
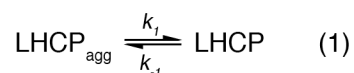
Previous work suggested that both the cpSRP43 and cpSRP54 subunits are necessary for the formation of a soluble transit complex with LHCP (12). Our results here strongly suggested that cpSRP43 is sufficient to bind and solubilize LHCP. The disparity between this and the previous studies could stem, in part, from the differences in experimental conditions. We have found that the activity and oligomeric state of cpSRP43 is sensitive to ionic strength. In buffers with low ionic strength (< 100 mM NaCl), which were typically used in previous studies, cpSRP43 exists as higher molecular weight complexes (Supplementary Figure 3.S1A). Under these low-salt conditions, cpSRP43 was sub-optimal for interacting with LHCP (Supplementary Figure 3.S1B and C). Presumably, the presence of cpSRP54 shifted the conformational equilibrium of cpSRP43 toward the more active monomeric state, and this likely contributed to the apparent requirement of cpSRP54 for interacting with LHCP under the previous assay conditions.

Kinetic simulations.

The Berkeley Madonna software was used to perform kinetic simulations for the different models of LHCP disaggregation (Figure 3.4C and D). For the passive model in Figure 3.4C, the following reactions were modeled (eq 1–2):



For the active mechanism in Figure 3.4D, the following reactions were modeled (eq 1–3):



in which LHCP_{agg} denotes the aggregated LHCP molecules, LHCP denotes a soluble LHCP monomer, $\text{LHCP}_{\text{cmplx}}$ denotes the cpSRP43-LHCP complex, and the rate constants are defined in Figure 3.3C and D. As this software considers only first-order or pseudo-first-order reactions, the concentration of cpSRP43 was varied by varying the values of k_2 and k_3 during the simulation. For the aggregation reaction (eq 1), the rate constant for LHCP aggregation (k_{-1}) was estimated to be 0.05 s^{-1} , based on the observation that LHCP aggregation is 70–80% complete within the first 15–20 seconds of mixing (Figure 3.1C, 3.4E, and Supplementary Figures 3.S3 and 3.S5). As the light scattering from aggregates was linear with LHCP concentration starting from $0.5 \text{ }\mu\text{M}$ (Figure 3.1C) indicating complete aggregate formation above this concentration, we assumed that the equilibrium favors aggregation by 100-fold under the experimental conditions. This gave the apparent rate of spontaneous disaggregation (k_1) of 0.0005 s^{-1} ; changing the value of k_1 from 0.00005 to 0.05 s^{-1} altered the time courses, but did not affect the conclusion that

the disaggregation rates are independent of cpSRP43 concentrations in the passive mechanism (Supplementary Figure 3.S2).

For the binding reaction between LHCP monomer and cpSRP43 (eq 2), we assumed an association rate constant (k_{on}) of $1 \times 10^6 \text{ M}^{-1}\text{s}^{-1}$, which is typical for bimolecular association between proteins. Varying the values of k_{on} from 10^6 to $10^8 \text{ M}^{-1}\text{s}^{-1}$ had no effect on the result of simulation (not shown). The value of k_{on} and the experimentally determined K_d value of $\sim 100 \text{ nM}$ (Figure 3.2A) were used to calculate the dissociation rate constant (k_{-2}). The apparent associating rate constants, k_2 , were calculated as $k_{on} \times [\text{cpSRP43}]$.

For the active disaggregation reaction (eq 3), we allowed the simulation program to fit the k_3 and k_{-3} values using experimental data. The values obtained from the simulation are comparable to the rate constants of disaggregation obtained from manual fitting of data (Supplementary Table 3.S1; see the next section).

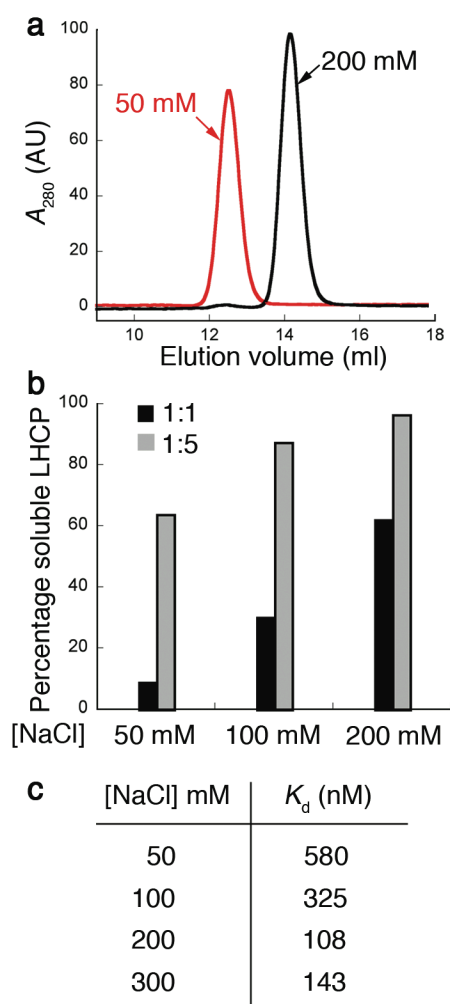
Analysis of rate constants for protein disaggregation.

The rate constants of protein disaggregation were obtained using several independent approaches. (i) The time courses of LHCP disaggregation in Figure 3.4E were fit to eq 1 in Methods to obtain the observed rate constants to reach equilibrium (k_{obsd}), which is the sum of forward disaggregation and reverse re-aggregation processes ($k_{\text{obsd}} = k_f + k_r$), and the equilibrium of each disaggregation reaction, which is determined by the relative magnitude of the disaggregation and re-aggregation processes [$K_{\text{obsd}} = k_f/(k_f + k_r)$]. Using these relationships, we calculated the net rate constants for the disaggregation process (k_f). (ii) In cases where a substantial amount of disaggregation

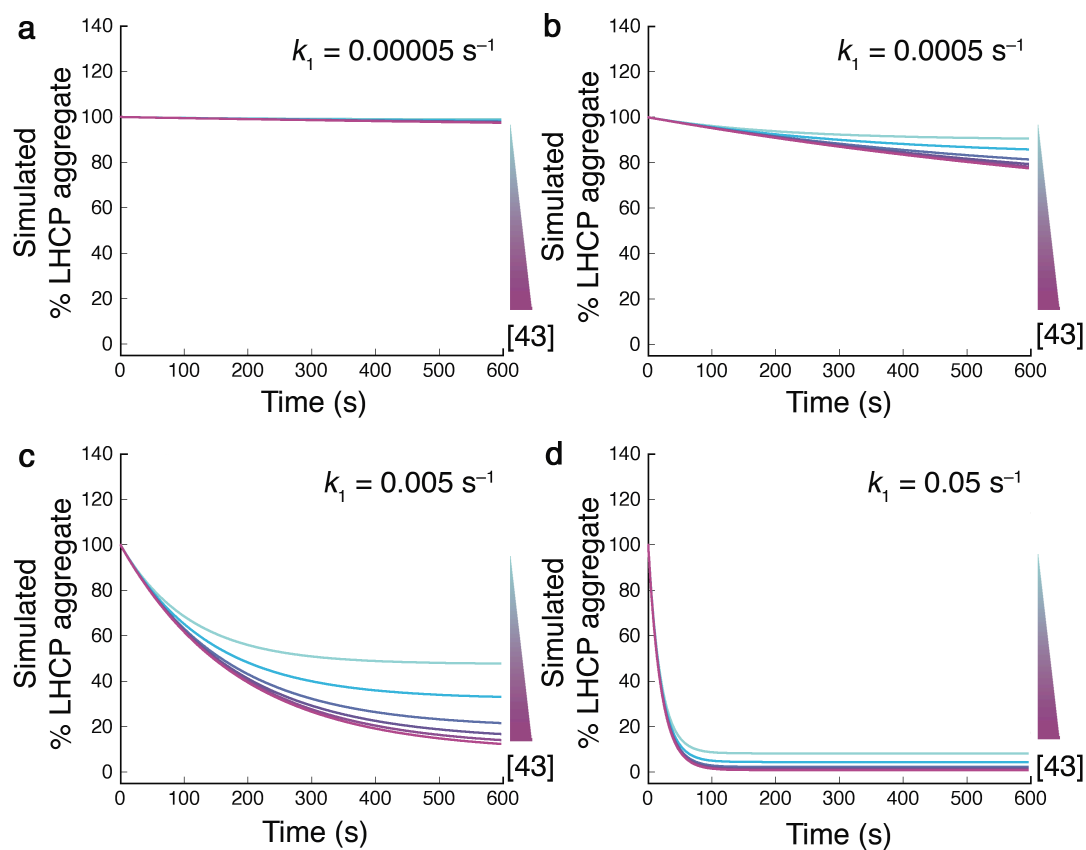
was achieved, the rate constants for the forward disaggregation reactions can also be estimated from the initial rates, since at earlier times the contribution from the reverse re-aggregation process is negligible. (iii) The Berkeley-Madonna program was used to fit the data in Figure 3.4E to the active remodeling mechanism in Figure 3.4D. The rate constants obtained from these different approaches were the same, within experimental error (Supplementary Table 3.S1).

Supplementary Table 3.S1 Comparison of disaggregation rate constants obtained from fits of data and simulation

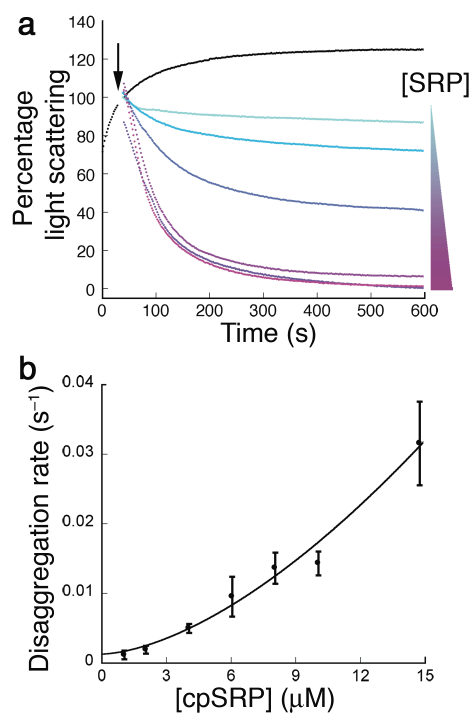
[cpSRP43] (μM)	k_f from manual fits of data (s^{-1})	k_3 from simulation (s^{-1})
2	0.0018	0.0023
4	0.0034	0.0041
6	0.0036	0.0050
8	0.0084	0.0084
10	0.0187	0.0180



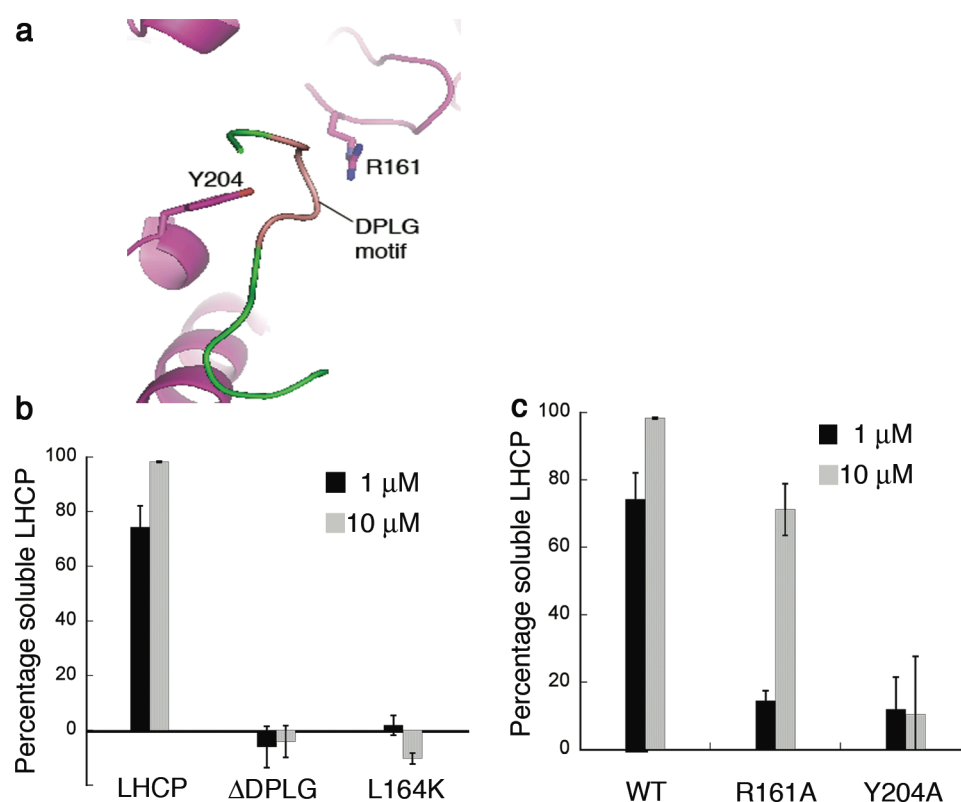
Supplementary Figure 3.S1 cpSRP43 is active at higher ionic strength, but is present as inactive multimeric forms at lower ionic strength. (A) cpSRP43 runs as a monomer on Superdex 200 in buffer containing 200 mM NaCl (black trace), but exhibits aberrant mobility in buffer containing 50 mM NaCl (red trace). (B) The amount of solubilized LHCP (1 μ M) at equilibrium in the presence of 1 μ M (black) or 5 μ M (gray) cpSRP43 in buffer with different salt concentrations. (C) List of the K_d values for the LHCP-cpSRP43 interaction, determined by fluorescence anisotropy, at different salt concentrations.



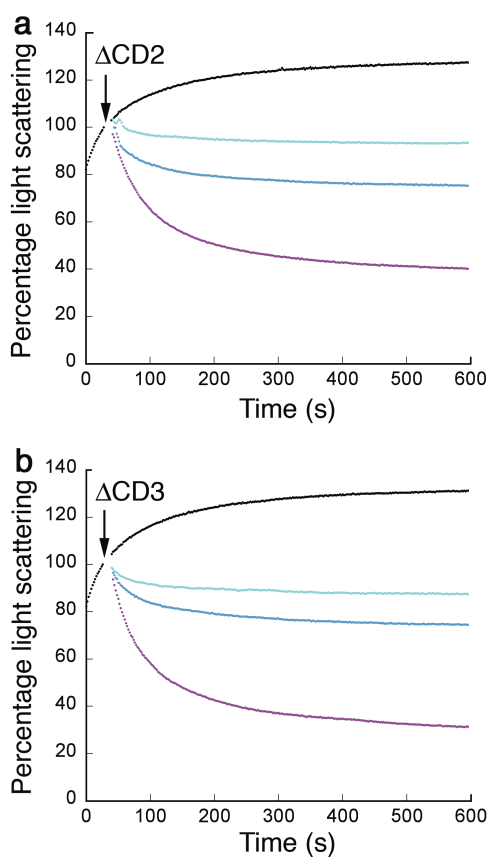
Supplementary Figure 3.S2 Kinetic simulations based on the passive mechanism in Figure 3.4C, which showed that the rates of disaggregation are independent of cpSRP43 concentration when the rates of spontaneous disaggregation (k_1) were varied over the range of $0.00005 - 0.05 \text{ s}^{-1}$.



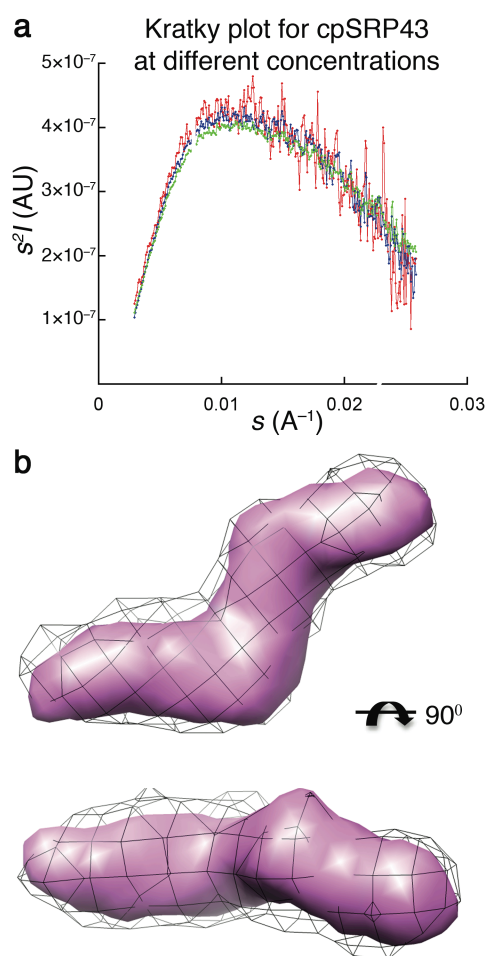
Supplementary Figure 3.S3 cpSRP actively reversed LHCP aggregation. (A) Time courses for disaggregation of LHCP (1 μM) at varying concentrations (2–10 μM) of cpSRP. The black arrow marks the time of cpSRP addition. (B) Concentration dependence of the forward rate constants of disaggregation reactions (k_f ; see text for derivation). The fits to eq 3 in Methods gave a Hill coefficient of 1.7.



Supplementary Figure 3.S4 Specific binding interactions between the L18 motif of LHCP and cpSRP are essential for chaperone activity. (A) The crystal structure of the L18 peptide (green) bound to the CD1–Ank4 fragment of cpSRP43 (magenta)(19). The DPLG motif is highlighted in pink. The two residues from cpSRP43 that make important contacts to this motif, R161 and Y204, are shown in sticks. (B) The amount of soluble LHCP (1 μM) or its mutants, ΔDPLG and L164K, at equilibrium in the presence of 1 μM (black) or 10 μM (gray) cpSRP. (C) The amount of soluble LHCP (1 μM) at equilibrium in the presence of 1 μM (black) or 10 μM (gray) cpSRP or its mutants, cpSRP-R161A and cpSRP-Y204A.



Supplementary Figure 3.S5 cpSRP43 deletion mutants, $\Delta CD2$ and $\Delta CD3$, can efficiently reverse LHCP aggregation. Time courses for disaggregation reactions by 2 μM (cyan), 4 μM (blue), and 8 μM (magenta) of cpSRP43 $\Delta CD2$ (A) and cpSRP43 $\Delta CD3$ (B).



Supplementary Figure 3.S6 SAXS analysis of full-length cpSRP43. (A) Experimental SAXS profiles in Kratky's representation at cpSRP43 concentrations of 50 μM (red), 100 μM (blue), and 200 μM (green). The agreement of the three curves indicated that no aggregation or interparticle interference occurred during the experiment. (B) Comparison of surface maps calculated from the dummy atom model in Figure 3.8B (pink shell) and from the docking model in Figure 3.8C (gray mesh).

References:

1. Balch, W. E., Morimoto, R.I., Dillin, A., and Kelly, J.F. (2008) Adapting proteostasis for disease intervention, *Science* 319, 916–919.
2. Hayer-Hartl, M., and Hartl, F.U. (2002) Molecular chaperones in the cytosol: from nascent chain to folded protein, *Science* 295, 1852–1858.
3. Chang, H.-C., Tang, Y.-C., Hayer-Hartl, M., and Hartl, F.U. (2007) Snapshot: Molecular chaperones, part I, *Cell* 128, 212–213.
4. Tang, Y.-C., Chang, H.-C., Hayer-Hartl, M., and Hartl, F.U. (2007) Snapshot: Molecular chaperones, part II, *Cell* 128, 412–413.
5. Doyle, S. M., and Wickner, S. (2008) Hsp104 and ClpB: protein disaggregating machines, *Trends Biochem. Sci.* 34, 40–48.
6. Doyle, S. M., Hoskins, J.R., and Wickner, S. (2007) Collaboration between the ClpB AAA+ remodeling protein and the DnaK chaperone system, *Proc. Natl. Acad. Sci. USA* 104, 11138–11144.
7. Randall, L. L., and Hardy, S.J.S. (2002) SecB, one small chaperone in the complex milieu of the cell, *Cell. Mol. Life Sci.* 59, 1617–1623.
8. Walton, T. A., Sandoval, C.M., Fowler, C.A., Pardi, A., and Sousa, M.C. (2009) The cavity-chaperone Skp protects its substrate from aggregation but allows independent folding of substrate domains, *Proc. Natl. Acad. Sci. USA* 106, 1772–1777.
9. Stefanovic, S., and Hegde, R.S. (2007) Identification of a targeting factor for posttranslational membrane protein insertion into the ER, *Cell* 128, 1147–1159.
10. Mihara, K., and Omura, T. (1996) Cytoplasmic chaperones in precursor targeting to mitochondria: the role of MSF and hsp70, *Trends Cell Biol.* 6, 104–108.
11. Schuenemann, D. (2004) Structure and function of the chloroplast signal recognition particle, *Curr. Genet.* 44, 295–304.
12. Schuenemann, D., Gupta, S., Persello-Cartieaux, F., Klimyuk, V. I., Jones, J. D. G., Nussaume, L., and Hoffman, N. E. (1998) A novel signal recognition particle targets light-harvesting proteins to the thylakoid membranes, *Proc. Natl. Acad. Sci. USA* 95, 10312–10316.
13. Groves, M. R., Mant, A., Kuhn, A., Koch, J., Dubel, S., Robinson, C., and Sinning, I. . (2001) Functional characterization of recombinant chloroplast signal recognition particle, *J. Biol. Chem.* 276, 27778–27786.
14. Tu, C.-J., Schuenemann, D., and Hoffman, N. E. (1999) Chloroplast FtsY, Chloroplast Signal Recognition Particle, and GTP are required to reconstitute the soluble phase of light-harvesting chlorophyll protein transport into thylakoid membranes, *J. Biol. Chem.* 274, 27219–27224.
15. Klimyuk, V. I., Persello-Cartieaux, F., Havaux, M., Contard-David, P., Schuenemann, D., Meierhoff, K., Gouet, P., Jones, J.D.G., Hoffman, N.E., and Nussaume, L. (1999) A chromodomain protein encoded by the arabidopsis CAO gene is a plant-specific component of the chloroplast signal recognition particle pathway that is involved in LHCP targeting, *The Plant Cell* 11, 87–99.
16. Eichacker, L. A., and Henry, R. (2001) Function of a chloroplast SRP in thylakoid protein export, *Biochim. Biophys. Acta* 1541, 120–134.

17. Jonas-Straube, E., Hutin, C., Hoffman, N.E., and Schuenemann D. (2001) Functional analysis of the protein-interacting domains of chloroplast SRP43, *J. Biol. Chem.* 276, 24654–24660.
18. Goforth, R. L., Peterson, E.C., Yuan, J., Moore, M.J., Kight, A.D., Lohse, M.B., Sakon, J., and Henry, R.L. (2004) Regulation of the GTPase cycle in post-translational signal recognition particle-based protein targeting involves cpSRP43, *J. Biol. Chem.* 279, 43077–43084.
19. Stengel, K. F., Holdermann, I., Cain, P., Robinson, C., Wild, K., and Sinning, I. (2008) Structural basis for specific substrate recognition by the chloroplast signal recognition particle protein cpSRP43, *Science* 321, 253–256.
20. Hermkes, R., Funke, S., Richter, C., Kuhlmann, J., and Schünemann, D. (2006) The α -helix of the second chromodomain of the 43 kDa subunit of the chloroplast signal recognition particle facilitates binding to the 54 kDa subunit, *FEBS Lett.* 580, 3107–3111.
21. Liu, Z., Yan, H., Wang, K., Kuang, T., Zhang, J., Gui, L., An, X., and Chang, W. (2004) Crystal structure of spinach major light-harvesting complex at 2.72 Å resolution, *Nature* 428, 287–292.
22. Cammarata, K., and Schmidt, G.W. (1992) In vitro reconstitution of a light-harvesting gene product: deletion mutagenesis and analyses of pigment binding, *Biochemistry* 31, 2779–2789.
23. Paulsen, H., Rumler, U., and Rudiger, W. (1990) Reconstitution of pigment-containing complexes from light-harvesting chlorophyll a/b-binding protein overexpressed in *Escherichia coli*, *Planta* 181, 204–211.
24. Delille, J., Peterson, E. C., Johnson, T., Morre, M., Kight, A., and Henry, R. (2000) A novel precursor recognition element facilitates posttranslational binding to the signal recognition particle in chloroplasts, *Proc. Natl. Acad. Sci.* 97, 1926–1931.
25. Tu, C. J., Peterson, E. C., Henry, R., and Hoffman, N. E. (2000) The L18 domain of light-harvesting chlorophyll proteins binds to chloroplast signal recognition particle 43, *J. Biol. Chem.* 275, 13187–13190.
26. Jaru-Ampornpan, P., Chandrasekar, S., Shan, S. (2007) Efficient interaction between two GTPases allows the chloroplast SRP pathway to bypass the requirement for an SRP RNA, *Mol Biol Cell.* 18, 2636–2645.
27. Yuan, J., Kight, A., Goforth, R.L., Moore, M., Peterson, E.C., Sakons, J., and Henry, R. (2002) ATP stimulates signal recognition particle (SRP)/FtsY-supported protein integration in chloroplasts, *J. Biol. Chem.* 277, 32400–32404.
28. Svergun, D. (1999) Restoring low resolution structure of biological macromolecules from solution scattering using simulated annealing, *Biophys. J.* 76, 2879–2886.
29. Svergun, D. I., Petoukhov, M.V. and Koch, M.H.J. . (2001) Determination of domain structure of proteins from X-ray solution scattering, *Biophys. J.* 80, 2946–2953.
30. Kozin, M., and Svergun, D.I. (2001) Automated matching of high and low resolution structural models, *J. Appl. Crystallogr.* 34, 33–41.

31. Volkov, V., and Svergun, D.I. (2003) Uniqueness of ab initio shape determination in small-angle scattering, *J. Appl. Crystallogr.* *36*, 860–864.
32. Wriggers, W., Milligan, R. A., and McCammon, J. A. (1999) Situs: a package for docking crystal structures into low-resolution maps from electron microscopy, *J. Struct. Biol.* *125*, 185–195.
33. Wriggers, W., and Chacon, P. (2001) Using Situs for the registration of protein structures with low-resolution bead models from X-ray solution scattering, *J. Appl. Crystallogr.* *34*, 773–776.
34. Pettersen, E., Goddard, T., Huang, C., Couch, G., Greenblatt, M., Meng, E., and Ferrin, E. (2004) UCSF Chimera—a visualization system for exploratory research and analysis, *J. Comput. Chem.* *13*, 1605–1612.
35. Oreb, M., Tews, I., and Schleiff, E. (2008) Policing Tic 'n' Toc, the doorway to chloroplasts, *Trends Cell Biol.* *18*, 19–27.
36. Li, X., Henry, R., Yuan, J., Cline, K., and Hoffman, N.E. (1995) A chloroplast homologue of the signal recognition particle subunit SRP54 is involved in the posttranslational integration of a protein into thylakoid membranes, *Proc. Natl. Acad. Sci. USA* *92*, 3789–3793.
37. Jansson, S. (1999) A guide to the Lhc genes and their relatives in arabidopsis, *Trends Plant Sci.* *4*, 236–240.
38. Barkow, S. R., Levchenko, I., Baker, T.A., and Sauer, R.T. (2009) Polypeptide translocation by the AAA+ ClpXP protease machine, *Chem Biol.* *16*, 605–612.
39. Tomoyasu, T., Mogk, A., Langen, H., Goloubinoff, P., and Bukau, B. (2001) Genetic dissection of the roles of chaperones and proteases in protein folding and degradation in the *Escherichia coli* cytosol, *Mol. Microbiol.* *40*, 397–413.
40. Mogk, A., Dougan, D., Weibezahn, J., Schlieker, C., Turgay, K., and Bukau, B. (2004) Broad yet high substrate specificity: the challenge of AAA+ proteins, *J. Struct. Biol.* *146*, 90–98.
41. Ali, M., Lipfert, J., Seifert, S., Herschlag, D., and Doniach, S. (2010) The ligand-free state of the TPP riboswitch: a partially folded RNA structure, *J. Mol. Biol.* *396*, 153–165.
42. Sivaraja, V., Kumar, T.K., Leena, P.S., Chang, A.N., Vidya, C., Goforth, R.L., Rajalingam, D., Arvind, K., Ye, J.L., Chou, J., Henry, R., and Yu, C. (2006) Three-dimensional solution structures of the chromodomains of cpSRP43, *J Biol Chem.* *280*, 41465–41471.
43. Goloubinoff, P., Mogk, A., Ben Zvi, A.P., Tomoyasu, T., Bukau, B. (1999) Sequential mechanism of solubilization and refolding of stable protein aggregates by a bichaperone network, *Proc. Natl. Acad. Sci. USA* *96*, 12732–12737.
44. Mogk, A., Schlieker, C., Friedrich, K.L., Schoenfeld, H.-J., Vierling, E., and Bukau, B. (2003) Refolding of substrates bound to small Hsps relies on a disaggregation reaction mediated most efficiently by ClpB/DnaK, *J. Biol. Chem.* *278*, 31033–31042.
45. Doyle, S. M., Shorter, J., Zolkiewski, M., Hoskins, J.R., Lindquist, S. and Wickner, S. (2007) Asymmetric deceleration of ClpB or Hsp104 ATPase activity unleashes protein-remodeling activity, *Nat Struct Mol Biol.* *14*, 114–122.

46. Schlothauer, T., Mogk, A., Dougan, D.A., Bukau, B., and Turgay, K. (2003) MecA, an adaptor protein necessary for ClpC chaperone activity, *Proc. Natl. Acad. Sci. USA* 100, 2306–2311.
47. Panse, V. G., Vogel, P., Trommer, W.E., and Varadarajan, R. (2000) A thermodynamic coupling mechanism for the disaggregation of a model peptide substrate by chaperone SecB, *J. Biol. Chem.* 275, 18698–18703.
48. Hachiya, N., Komiya, T., Alam, R., Iwahashi, J., Sakaguchi, M., Omura, T., and Mihara, K. (1994) MSF, a novel cytoplasmic chaperone which functions in precursor targeting to mitochondria, *EMBO J.* 13, 5146–5154.
49. Komiya, T., Hachiya, N., Sakaguchi, M., Omura, T., Mihara, K. (1994) Recognition of mitochondria-targeting signals by a cytosolic import stimulation factor, MSF, *J Biol Chem.* 269, 30893–30897.